Increasing precipitation volatility in twenty-first-century California

Daniel L. Swain [1,2]*, Baird Langenbrunner[3,4], J. David Neelin[3] and Alex Hall[3]

Mediterranean climate regimes are particularly susceptible to rapid shifts between drought and flood—of which, California's rapid transition from record multi-year dryness between 2012 and 2016 to extreme wetness during the 2016–2017 winter provides a dramatic example. Projected future changes in such dry-to-wet events, however, remain inadequately quantified, which we investigate here using the Community Earth System Model Large Ensemble of climate model simulations. Anthropogenic forcing is found to yield large twenty-first-century increases in the frequency of wet extremes, including a more than threefold increase in sub-seasonal events comparable to California's 'Great Flood of 1862'. Smaller but statistically robust increases in dry extremes are also apparent. As a consequence, a 25% to 100% increase in extreme dry-to-wet precipitation events is projected, despite only modest changes in mean precipitation. Such hydrological cycle intensification would seriously challenge California's existing water storage, conveyance and flood control infrastructure.

Mediterranean climate regimes are renowned for their distinctively dry summers and relatively wet winters—a globally unusual combination[1]. Such climates generally occur near the poleward fringe of descending air in the subtropics, where semi-permanent high-pressure systems bring stable conditions during most of the calendar year[2]. Here, the majority of precipitation occurs during the passage of transient storm events during a short rainy season[3]—a distinct seasonality brought about by an equatorward shift in the mid-latitude storm track during winter[4]. The same factors that imbue such regions with their temperate mean climate state, however, are also conducive to dramatic swings between drought and flood[4–6]. Subtle year-to-year jetstream shifts can generate disproportionately large precipitation variability[7]—yielding highly non-uniform precipitation distributions[8] and increasing the intrinsic likelihood of hydroclimatic extremes[4,9]. These effects are often amplified in California, where a combination of complex topography and over 1,000 km of latitudinal extent yield a great diversity of microclimates within the broader 'dry summer' regime[1].

California's rapid shift from severe drought to abundant precipitation (and widespread flooding) during the 2016–2017 winter[10] offers a compelling example of one such transition in a highly populated, economically critical and biodiverse region[11,12]. Immediately following one of the most intense multi-year droughts on record between 2012 and 2016 (refs [13–15]), the state experienced several months of heavy precipitation associated with an extraordinarily high number of atmospheric river storms during November–March 2016–2017 (ref. [10]). While the heaviest precipitation was concentrated in northern Sierra Nevada watersheds, hundreds of roads throughout California were damaged by floodwaters and mudslides (including a major bridge collapse)[16]. In February 2017, heavy runoff in the Feather River watershed contributed to the failure of the Oroville Dam's primary spillway—culminating in a crisis that forced the emergency evacuation of nearly a quarter of a million people[17].

Previous studies focusing on future changes in California precipitation have generally reported modest[18–20] (and/or uncertain) changes in regional mean precipitation[7,20]. More recent work,

however, has suggested an increased likelihood of wet years[20–23] and subsequent flood risk[9,24] in California—which is consistent with broader theoretical and model-based findings regarding the tendency towards increasing precipitation intensity[25] in a warmer (and therefore moister) atmosphere[26,27]. Meanwhile, while evidence shows that anthropogenic warming has contributed to an increased risk of California drought via increasing temperatures[28,29] and increased frequency of seasonally persistent high-pressure ridges[8,14,30,31], attribution studies focusing directly on precipitation have yielded mixed results[18,32]. Contributing additional uncertainty are climate model simulations suggesting that the boundary between mean subtropical drying and mid-latitude wetting will probably occur over California[33], potentially yielding strong latitudinal gradients in the precipitation response. Thus, while there is already substantial evidence that climate change will induce regional hydroclimatic shifts, a cohesive picture has yet to emerge—presenting serious challenges to decision-makers responsible for ensuring the resilience of California's water infrastructure[11].

Importance of large ensemble approach

We use specific flood and drought events from California's history as baselines for exploring the changing character of precipitation extremes. Our use of a large ensemble of climate model simulations[34]—the Community Earth System Model Large Ensemble (CESM-LENS)—allows us to directly quantify changes in large-magnitude extremes. This approach offers a substantial advantage over traditional climate model experiments, which yield too small a sample size of statistically rare extreme events to draw robust inferences without making assumptions regarding the underlying precipitation distribution[35]. By selecting a wide range of wet, dry and dry-to-wet transition (that is, 'whiplash') events informed by historical analogues, we aim to provide a comprehensive perspective on the changing risks of regional hydroclimate extremes in a manner directly relevant to climate adaptation and infrastructure planning efforts.

[1]Institute of the Environment and Sustainability, University of California, Los Angeles, Los Angeles, CA, USA. [2]The Nature Conservancy, Arlington, VA, USA. [3]Department of Atmospheric and Oceanic Sciences, University of California, Los Angeles, Los Angeles, CA, USA. [4]Department of Earth System Science, University of California, Irvine, Irvine, CA, USA. *e-mail: dlswain@ucla.edu

We assess simulated changes in the frequency of California precipitation extremes caused by increasing atmospheric greenhouse gas concentrations. Our overall approach is to (1) determine approximate frequency of occurrence for each event of interest based on direct observations or historical accounts, (2) calculate the magnitude of events within a preindustrial control climate model simulation that occur with comparable frequency to those observed and (3) quantify subsequent frequency changes in similar events under a scenario of continued growth in greenhouse gas concentrations.

We focus on changes in frequency of precipitation events exceeding particular thresholds for two key reasons. First, historical civil engineering and risk management practices have been predicated on a largely stationary climate[36], and the majority of existing water storage and conveyance structures have been constructed under such assumptions. Second, a frequency-based approach also offers the considerable advantage of implicit climate model bias correction. While all global climate models exhibit some degree of mean precipitation bias in topographically complex California[9], the use of a long preindustrial control simulation to define return interval thresholds allows us to make internally consistent comparisons between simulated precipitation distributions at different levels of radiative forcing. We can therefore select CESM-LENS precipitation thresholds corresponding to approximate return intervals of real-world historical events, which serve as analogues for impacts.

Large increase in extreme wet-event frequency

We find large, statistically robust increases in the simulated frequency of extremely heavy precipitation events on multiple timescales. All of California experiences a 100–200% increase in the occurrence of very high cumulative seasonal precipitation (of a magnitude comparable to the 2016–2017 season on a statewide basis) by the end of the twenty-first century (Fig. 1). This simulated increase in seasonal wet extremes across California is part of a broader regional increase extending across the Pacific coast. Seasonal precipitation of this magnitude (equivalent to that associated with the 25 year preindustrial control (PIC) return interval) has only occurred a handful of times over the lifespan of California's modern water infrastructure. It represents a rarely exceeded but not unprecedented threshold, for which there are analogues in the recent historical record.

We note, however, that California's most severe floods do not necessarily coincide with its wettest winters. Instead, regional flood events are more directly linked to persistent storm sequences on sub-seasonal timescales, which are capable of bringing a significant fraction of annual average precipitation over a brief period[3,6,37]. Thus, to better characterize changes in the frequency of such 'high consequence, low probability' precipitation events, we use a sub-seasonal threshold motivated by the extraordinary sequence of 'atmospheric river' storms that brought extremely severe flooding to much of California during the winter of 1861–1862 (refs [38,39]). We define 40 day precipitation accumulations exceeding the 200 year preindustrial return interval as a measure of occurrences comparable to this benchmark event (see Methods).

Given the severe impacts even one such occurrence would have on California's existing infrastructure and population centres[40], we assess cumulative twenty-first-century risk beginning in the present winter season (2017–2018). Figure 2 shows that at least two-thirds (66.66%) of LENS ensemble members simulate two or more 1862-magnitude events over this interval across virtually all of California—which represents a dramatic increase in likelihood relative to preindustrial simulations (where, by definition, the cumulative 83 year likelihood of a single occurrence is less than 50%). Strikingly, these findings suggest that California's major urban centres (including San Francisco and Los Angeles) are more likely than not to experience at least one such extremely severe storm sequence between 2018 and 2060 (Fig. 2b,c) on a business-as-usual emissions
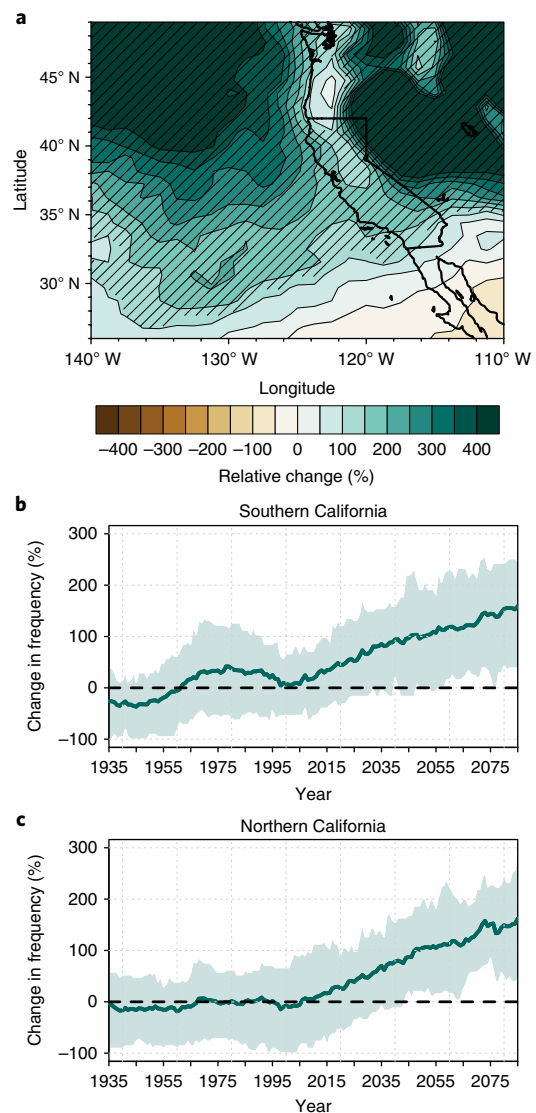
Fig. 1 | Change in frequency of extremely wet seasons. a, Relative (%) change in frequency of extremely wet seasons (meeting or exceeding the 25 year PIC return interval for November–March precipitation) at end of the twenty-first century (2070–2100, RCP8.5 forcing) relative to the preindustrial era (1850 forcing). Cross-hatching signifies 90% statistical confidence ($P < 0.10$) in robustness of frequency shifts across the full 40-member CESM-LENS ensemble. **b,c**, Time series showing relative (%) change in frequency of extremely wet seasons in each year from 1935 to 2085 (solid green curve) for a cluster of grid boxes in Southern California (**b**) and Northern California (**c**). Data are smoothed over 30 year intervals, and the green shaded range encompasses two-thirds (66.66%) of the CESM-LENS ensemble spread (that is, the 16.66th and 83.33th percentile bounds). Dashed black horizontal lines in **b** and **c** denote zero change in frequency.

trajectory. On a statewide basis, the overall frequency of 1862-magnitude events increases on the order of 300–400% by the end of the twenty-first century (Supplementary Fig. 2).

These increases in extreme wet-event frequency across the large ensemble emerge in an essentially monotonic fashion throughout most of California beginning between around 2010–2020 for both seasonal (25 year) wet events (Supplementary Fig. 3a) and sub-seasonal (200 year) wet events (Supplementary Fig. 3b). In addition to the robust ensemble-mean signal by mid-to-late century for both
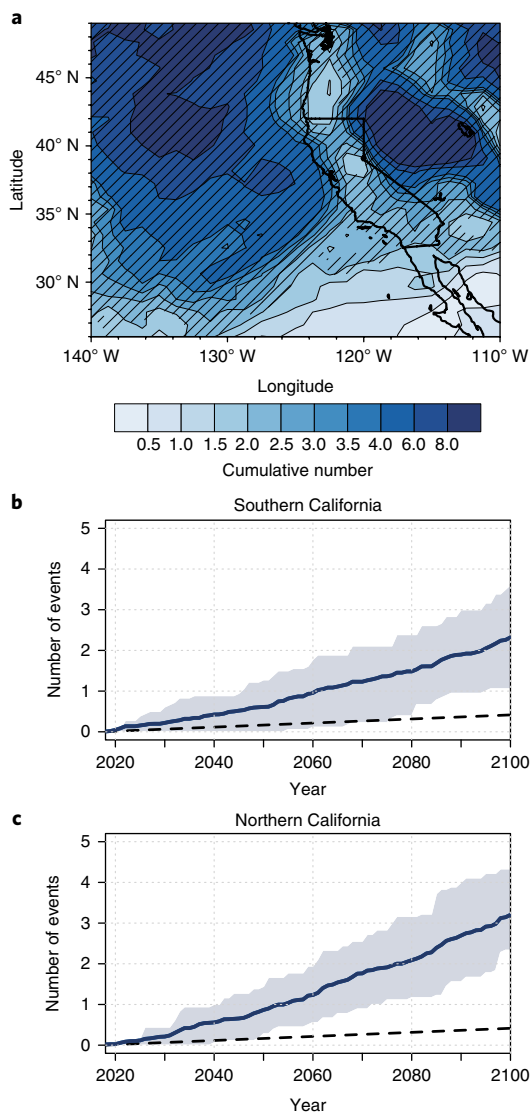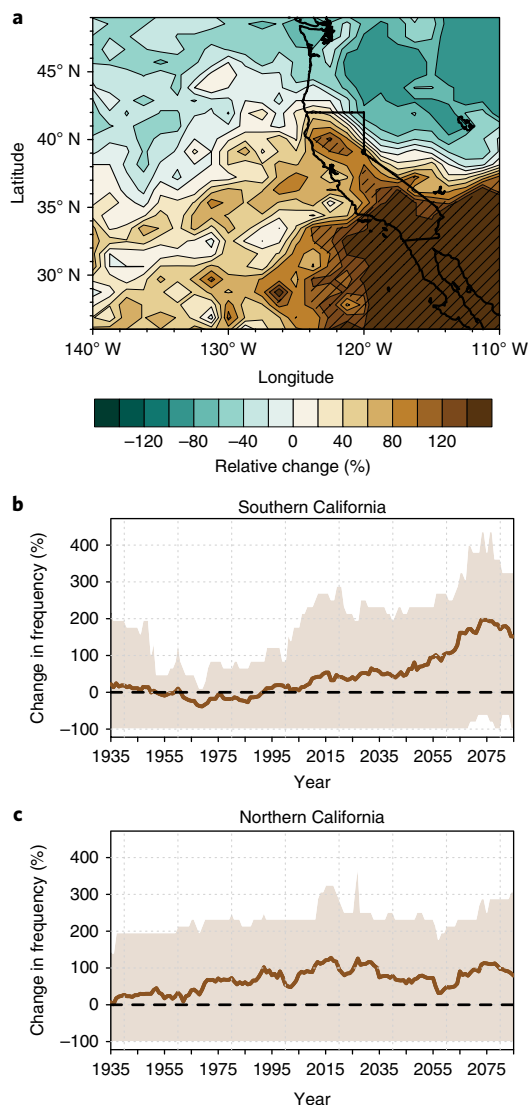
Fig. 2 | Cumulative occurrence of extremely wet sub-seasonal storm sequences. a, Cumulative number of extremely wet sub-seasonal storm sequences (meeting or exceeding the 200 year PIC return interval for cumulative 40 day precipitation) occurring in CESM-LENS between 2018 and 2100 under RCP8.5 forcing. Cross-hatching signifies regions where at least two-thirds (66.66%) of CESM-LENS ensemble members simulate two or more such occurrences. **b,c**, Time series showing cumulative number of extremely wet sub-seasonal storm sequences during 2018–2100 (solid blue curve) for a cluster of grid boxes in Southern California (**b**) and Northern California (**c**). Blue shaded range encompasses two-thirds (66.66%) of the CESM-LENS ensemble spread (that is, the 16.66th and 83.33th percentile bounds). Dashed black curve depicts baseline cumulative occurrence over an equivalent time interval assuming constant preindustrial climate forcings.

Fig. 3 | Change in frequency of extremely dry seasons. a, Relative (%) change in frequency of extremely dry seasons (meeting or falling below the 100 year PIC return interval for low November–March precipitation) at end of the twenty-first century (2070–2100, RCP8.5 forcing) relative to the preindustrial era (1850 forcing). Cross-hatching signifies 90% statistical confidence ($P < 0.10$) in robustness of frequency shifts across the full 40-member CESM-LENS ensemble. **b,c**, Time series showing relative (%) change in frequency of extremely dry seasons in each year 1935–2085 (solid brown curve) for a cluster of grid boxes in Southern California (**b**) and Northern California (**c**). Data are smoothed over 30 year intervals, and the brown shaded range encompasses two-thirds (66.66%) of the CESM-LENS ensemble spread (that is, the 16.66th and 83.33th percentile bounds). Dashed black horizontal lines in **b** and **c** denote zero change in frequency.

extreme wet events, these results also imply that an increased likelihood of large precipitation accumulations relative to a preindustrial climate may already exist. However, we note that a handful of outlying ensemble members suggest a chance that internal variability could delay emergence of an attributable signal by several decades (Fig. 1b,c and Fig. 2b,c).

Shifts in extreme dry-event frequency

The simulated frequency of extremely dry years also increases across nearly all of California (Fig. 3). An increased likelihood of these

extremely dry rainy seasons (that is, exceeding the 100 year return interval, analogous to the 1976–1977 drought and slightly drier than 2013–2014) first emerges weakly across portions of the state as early as the 1980s, before emerging in a statistically robust manner across Northern California around 2010–2020 and Southern California later in the century (around 2060; Supplementary Fig. 4a). Notable are especially large increases (>140%) in frequency that occur across Southern California after 2050 (Fig. 3b and Supplementary Fig. 4a), though we emphasize that substantial increases on the order of +80% extend across most of Northern California. Except

for southernmost California, much of this increased risk emerges during the twentieth and early twenty-first centuries (Fig. 3b,c and Supplementary Fig. 4a)—suggesting that the likelihood of individual dry seasons may already be increased relative to the preindustrial period.

In contrast, changes in the occurrence of extremely dry consecutive years analogous to the record-low 3 year cumulative statewide precipitation observed during 2013–2015 (100 year return interval on a 3 year basis) exhibit a more complex temporal and spatial structure (Supplementary Fig. 4b). By the end of the twenty-first century, only far southern California experiences a robust increase in the frequency of consecutively dry seasons (Supplementary Fig. 2), while the rest of California does not experience statistically significant changes. Further analysis shows that this divergence between single and consecutive dry-season frequency shifts arises from the increased pace of future wet-year increases relative to dry-year increases, which is especially pronounced across Northern California (Supplementary Fig. 5c). These findings suggest that future multi-year droughts in California may exhibit an increased propensity to be interrupted by very wet interludes.

Emergence of 'precipitation whiplash' signal

Given the large simulated increase in the frequency of both dry and wet extremes, we test whether the frequency of rapid transitions between dry and wet conditions—similar to the precipitation whiplash that occurred between the recent 2012–2016 drought and 2016–2017 floods—also increases. For the purposes of this study, we define precipitation whiplash as the occurrence of two consecutive years during which rainy season (November–March) precipitation falls under the PIC 20th percentile (in the first year) and subsequently exceeds the PIC 80th percentile (in the following year). Figure 4 confirms such an increase during the twenty-first century throughout California. We report a strong latitudinal gradient in the year-to-year (interannual) whiplash response to anthropogenic forcing, ranging from an ~100% increase across Southern California to an ~25% increase in Northern California (Fig. 4a). These whiplash increases first emerge in the south relatively early in the twenty-first century (2010–2020) before spreading progressively northward in a statistically robust manner in the following decades (especially after 2050; Supplementary Fig. 5). We also investigate changes in month-to-month (sub-seasonal) precipitation variability during the canonical wet season. We report modest but widespread increases of 20–30% across a broad swath of the northeastern Pacific region, again extending across all of California (Supplementary Fig. 2c).

Together, these shifts represent a marked increase in both the interannual and intraseasonal variability of precipitation, especially in Southern California—which is noteworthy for two distinct reasons. First, natural precipitation variability in this region is already large[6], and projected future whiplash increases would amplify existing swings between dry and wet years (and between dry and wet months within the rainy season). Second, the robust emergence of a precipitation whiplash signal across a wide range of timescales (Fig. 4 and Supplementary Fig. 2c) is remarkable, as large-scale atmospheric variability over the North Pacific relevant to California precipitation is dominated by different physical processes and associated remote teleconnections on sub-seasonal (for example, the Madden–Julian Oscillation[41]) and interannual (for example, El Nino–Southern Oscillation (ENSO)[42]) timescales.

## Increasingly sharp seasonality of California wet season

We find a distinct sharpening of California's future mean seasonal cycle (Fig. 5). While winter mean precipitation increases across most of California, mean precipitation during autumn (September–November) and especially spring (March–May) decreases nearly everywhere, which is consistent with previous findings from the Coupled Model Intercomparison Project Phase
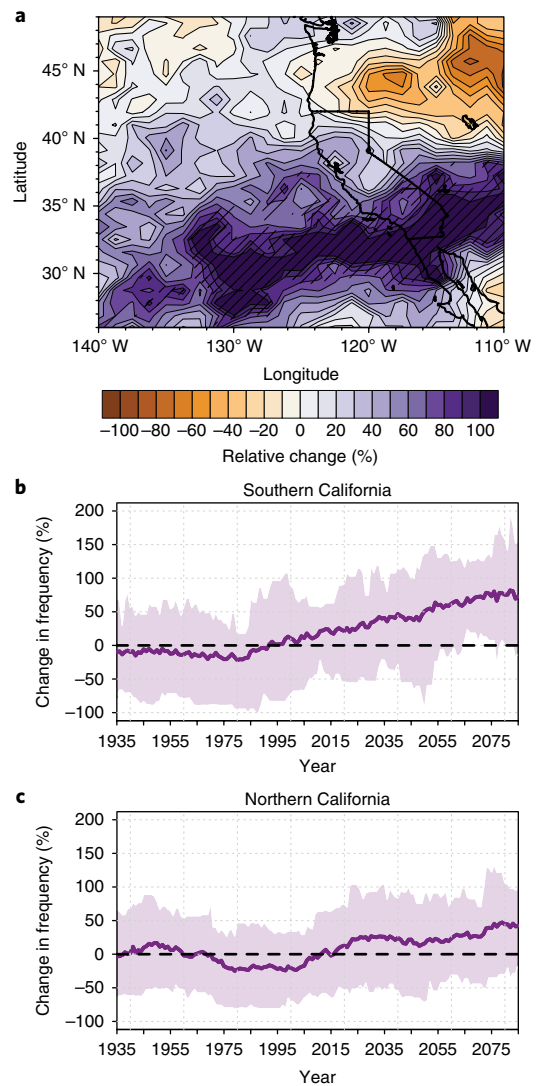
Fig. 4 | Change in frequency of precipitation whiplash events. a, Relative (%) change in frequency of dry-to-wet precipitation whiplash events (years with November–March precipitation at or above the 80th preindustrial percentile immediately followed by a year with precipitation below the 20th preindustrial percentile) at end of the twenty-first century (2070–2100, RCP8.5 forcing) relative to the preindustrial era (1850 forcing). Cross-hatching signifies 90% statistical confidence ($P < 0.10$) in robustness of frequency shifts across the full 40-member CESM-LENS ensemble. **b,c**, Time series showing relative (%) change in frequency of whiplash events in each year 1935–2085 (solid purple curve) for a cluster of grid boxes in Southern California (**b**) and Northern California (**c**). Data are smoothed over 30 year intervals, and the purple shaded range encompasses two-thirds (66.66%) of the CESM-LENS ensemble spread (that is, the 16.66th and 83.33th percentile bounds). Dashed black horizontal lines in **b** and **c** denote zero change in frequency.

5 (CMIP5) ensemble[43]. This striking contrast between the drying marginal and wetting core rainy season months results in a large ensemble-mean increase (35% to 85% from north to south) in the ratio of overall wet season precipitation falling between November and March relative to cumulative precipitation during the four months of September, October, April and May (Fig. 5). This increase in sharpness of precipitation seasonality suggests that the already distinct contrast between California's long, dry summers and relatively brief, wet winters will probably become even more
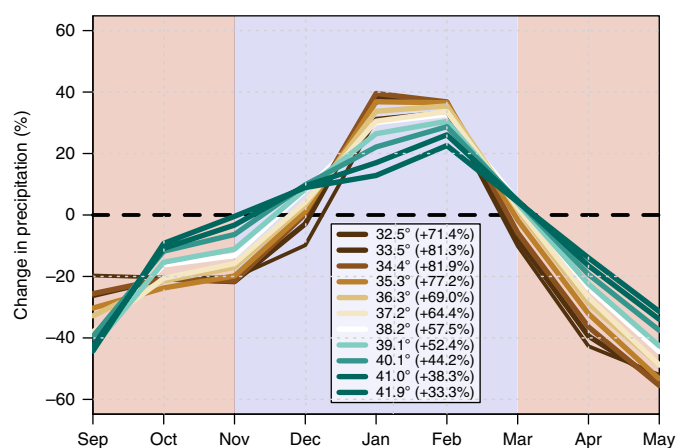
Fig. 5 | Shifts in precipitation seasonality. Relative changes in CESM-LENS monthly mean precipitation at the end of the twenty-first century (2070–2100) as a percent of the PIC climatology for each calendar month for a range of latitudes spanning the California coast. Percentages in the legend denote relative changes in mean 'seasonal sharpness' at each latitude, defined as the ratio between precipitation falling during the core rainy season (November–March; blue background shading) to that cumulatively falling during the marginal rainy season (September–October, April–May; red background shading). Curves are colour coded by latitude (and therefore by mean seasonal precipitation, which increases monotonically with latitude). Dashed black horizontal line denotes zero change in magnitude.

pronounced during the twenty-first century. While a comprehensive assessment is beyond the scope of this study, we note that autumn and spring drying trends have recently begun to emerge in observations across California (Supplementary Fig. 7)—suggesting that the projected concentration of precipitation into an even narrower season may already be underway.

Increase in extremes despite modest mean change

The substantial increases in California precipitation extremes over a wide range of timescales and intensities occur despite only modest changes in rainy season mean precipitation. By the end of the twenty-first century, the CESM-LENS ensemble mean depicts modest cool-season wetting over the northern portion of the state (<20–30%; Fig. 5), with little change in the south (~0%; Supplementary Fig. 6)—similar to the CMIP5 multi-model ensemble-mean response (Supplementary Fig. 6). Yet over the same interval, the frequencies of both extreme dry seasons and whiplash events increase by over 50% over much of the state (Figs. 3 and 4), and the frequency of extreme wet events increases by well over 100% nearly everywhere (Fig. 1 and Supplementary Fig. 2). This remarkable divergence between simulated future mean and extreme climate is especially pronounced across Southern California. For example: simulated mean precipitation in Southern California exhibits little trend by the end of the twenty-first century (Supplementary Fig. 5), despite an ~200% increase in extremely dry seasons (Fig. 3), an ~150% increase in extremely wet seasons (Fig. 1), a >500% increase in extreme sub-seasonal precipitation events (Fig. 2 and Supplementary Fig. 2) and an ~75% increase in year-to-year whiplash (Fig. 4). Importantly, these findings suggest that lingering uncertainty regarding the magnitude (and even sign) of regional mean precipitation change does not preclude statistically robust conclusions regarding changes in precipitation extremes.

Changes in processes responsible for extremes

We confirm that simulated large-scale atmospheric circulation patterns associated with California wet and dry extremes are

substantially similar to those observed historically (Supplementary Fig. 12). Wet years are linked to strong low-pressure anomalies over the northeastern Pacific Ocean (Fig. 6a), with downstream enhancement of the storm track just west of California[7,14]. Dry years coincide with seasonally persistent high pressure extending across the northeastern Pacific (Fig. 6d), which reinforces the climatological mean ridge along the West Coast[14] and prevents storms from reaching California[44].

We find that future (representative concentration pathway 8.5 (RCP8.5)) wet and dry years are linked to broadly similar atmospheric circulation anomalies as those in the past (PIC; Fig. 6b,e)—suggesting that the spatial character of large-scale features driving California precipitation extremes may remain relatively stationary. However, given that subtle storm track perturbations can yield disproportionately large shifts in California precipitation[7,14,20], we note two potentially important differences between the RCP8.5 and PIC composites. In future wet years, low pressure over the North Pacific is deeper to the west of California (Fig. 6b), which previous work using models in the CMIP5 experiment has suggested is linked to a localized eastward extension of the jetstream[7,20]. In RCP8.5 dry years, atmospheric pressure anomalies in the immediate vicinity of California are similar to PIC dry years (Fig. 6e), but are higher in adjacent regions—suggesting a broader, more longitudinally oriented atmospheric ridge pattern and subsequent poleward storm track shift.

We also report large increases in atmospheric water vapour during both future wet and dry years. While this moistening is not in itself surprising—given the well-understood thermodynamic consequences of the Clausius–Clapeyron relation[45]—we point out that RCP8.5 dry years occur in an atmosphere moister than that during even the wettest years of the PIC simulation (Fig. 6c,f). The fact that California dry years occur more frequently (Fig. 3) suggests that simulated (thermodynamic) moistening must be counteracted (at least periodically) by changes in the frequency and/or intensity of atmospheric circulation patterns that prevent precipitation-bearing storms from reaching California, such as persistent high-pressure systems[14] or transient poleward shifts in the East Pacific storm track[7]. Conversely, the (thermodynamic) increase in water vapour would probably reinforce the (dynamic) effect of deeper North Pacific low pressure during wet years—which may underlie the relatively larger simulated increase in extreme wet-event frequency (versus dry-event frequency). Nonetheless, we emphasize that further work is necessary to better understand underlying changes in both remote (tropical[31,44] and Arctic teleconnections[46–48]) and regional-scale (that is, atmospheric rivers[9] and orographic precipitation) influences.

Societal implications of hydrological intensification

Collectively, our findings suggest that anthropogenic warming will bring about large increases in the frequency of California hydroclimatic extremes similar or greater in magnitude to those that have historically caused widespread disruption. These changes in the character of California precipitation emerge in a large single-model ensemble despite only modest trends in mean precipitation—strongly suggesting that the region's already variable year-to-year climate is likely to become even more volatile. Historically observed impacts of droughts and floods may in many cases offer reasonable analogues for the human and environmental impacts of future events of a similar magnitude, but increasingly wide swings between dry and wet conditions will threaten to upset the already precarious balance between competing flood control and water storage imperatives in California.

Moreover, we report a substantial increase in the projected risk of extreme precipitation events exceeding any that have occurred over the past century—meaning that such events would be unprecedented in California's modern era of extensive water infrastructure. Few of the dams, levees and canals that currently protect millions living in California's flood plains and facilitate the movement of
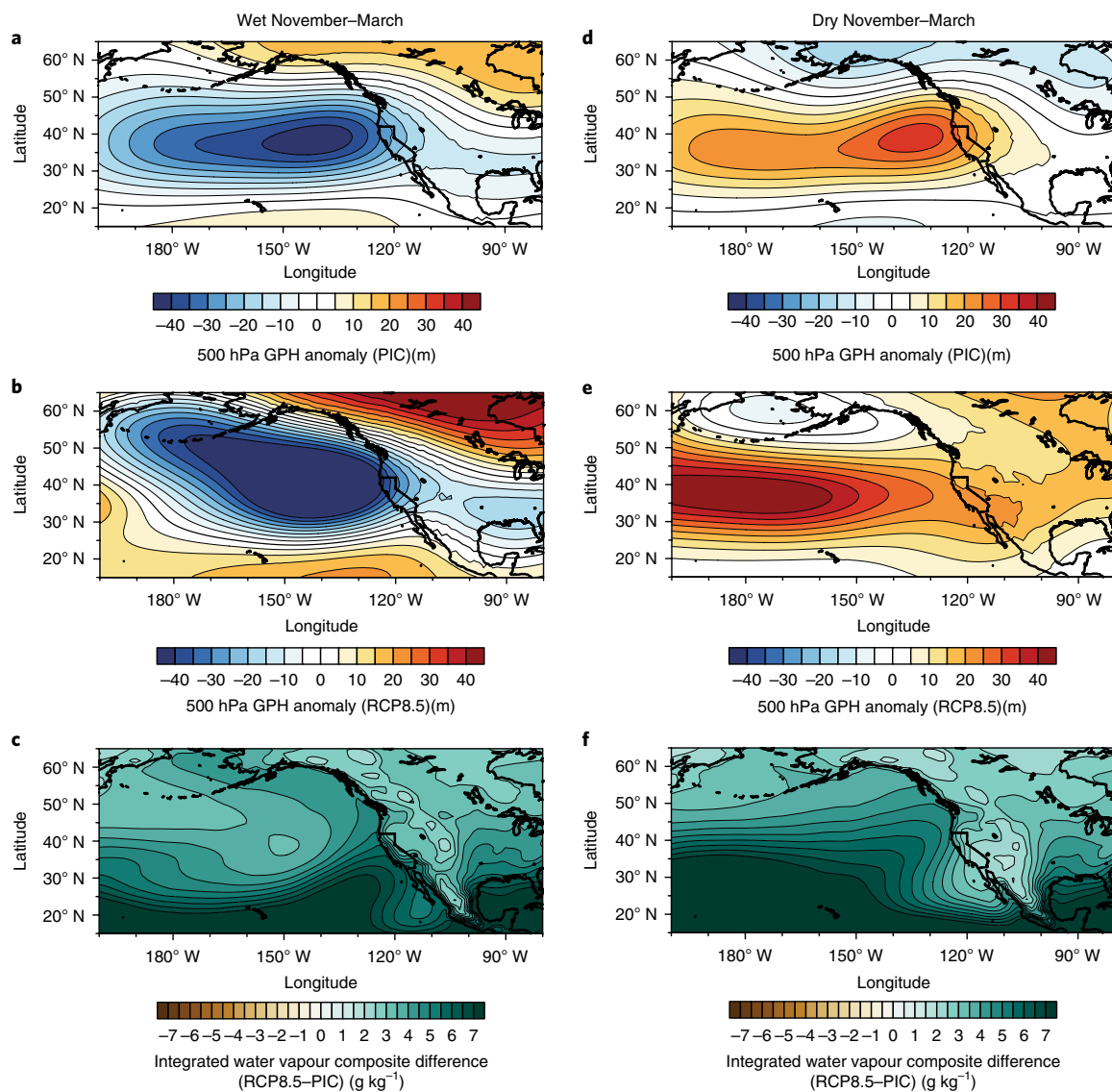
Fig. 6 | Large-scale atmospheric conditions linked to California precipitation extremes. a,d, Composite maps depicting anomalies in November–March 500 hPa GPH during wet (80th percentile, left column) and dry (20th percentile, right column) March–November seasons in the CESM-LENS simulation. **b,e,** RCP8.5 (2081–2100) composite anomaly patterns for GPH (see Methods). **c,f,** Difference between RCP8.5 (2081–2100) and PIC composite anomaly patterns for column-integrated water vapour.

water from Sierra Nevada watersheds to coastal cities have been tested by a deluge as severe as the extraordinary 1861–1862 storm sequence—a repeat of which would probably lead to considerable loss of life and economic damages approaching a trillion dollars[39,40]. Our results suggest that such an event is more likely than not to occur at least once between 2018 and 2060, and that multiple occurrences are plausible by 2100 on a business-as-usual emissions trajectory. Therefore, recognizing that risks associated with hydroclimatic extremes may rise more rapidly than the gradual projected shift in regional mean precipitation might otherwise suggest will be a critical step in ensuring resilience amid a warming climate.

Methods

Methods, including statements of data availability and any associated accession codes and references, are available at https://doi.org/10.1038/s41558-018-0140-y.

References

1. Kottek, M., Grieser, J., Beck, C., Rudolf, B. & Rubel, F. World map of the Köppen-Geiger climate classification updated. *Meteorol. Z.* **15**, 259–263 (2006).
2. Karnauskas, K. B. & Ummenhofer, C. C. On the dynamics of the Hadley circulation and subtropical drying. *Clim. Dynam.* **42**, 2259–2269 (2014).
3. Dettinger, M. Atmospheric rivers as drought busters on the US West Coast. *J. Hydrometeorol.* **14**, 1721–1732 (2013).
4. Stephen, H. S., Terry, L. R. & Michael, D. M. *Encyclopedia of Climate and Weather* (Oxford Univ. Press, New York, 2011).
5. Horton, D. et al. Contribution of changes in atmospheric circulation patterns to extreme temperature trends. *Nature* **522**, 465–469 (2015).
6. Dettinger, M. D., Ralph, F. M., Das, T., Neiman, P. J. & Cayan, D. R. Atmospheric rivers, floods and the water resources of California. *Water* **3**, 445–478 (2011).
7. Langenbrunner, B., Neelin, J. D., Lintner, B. R. & Anderson, B. T. Patterns of precipitation change and climatological uncertainty among CMIP5 models, with a focus on the midlatitude Pacific storm track. *J. Clim.* **28**, 7857–7872 (2015).
8. Swain, D. et al. The extraordinary California drought of 2013/2014: character, context, and the role of climate change. *Bull. Am. Meteorol. Soc.* **95**, S3–S7 (2014).

9. Dettinger, M. Historical and future relations between large storms and droughts in California. *San Francisco Estuary Watershed Sci.* **14**, 1 (2016).
10. Wang, S. Y. S., Yoon, J.-H., Becker, E. & Gillies, R. California from drought to deluge. *Nat. Clim. Change* **7**, 465–468 (2017).
11. Swain, D. A tale of two California droughts: lessons amidst record warmth and dryness in a region of complex physical and human geography. *Geophys. Res. Lett.* **42**, 9999–10003 (2015).
12. Cowling, R. M., Rundel, P. W., Lamont, B. B., Kalin Arroyo, M. & Arianoutsou, M. Plant diversity in Mediterranean-climate regions. *Trends Ecol. Evol.* **11**, 362–366 (1996).
13. Griffin, D. & Anchukaitis, K. J. How unusual is the 2012–2014 California drought?. *Geophys. Res. Lett.* **41**, 9017–9023 (2014).
14. Swain, D., Horton, D., Singh, D. & Diffenbaugh, N. Trends in atmospheric patterns conducive to seasonal precipitation and temperature extremes in California. *Sci. Adv.* **2**, e1501344 (2016).
15. Robeson, S. Revisiting the recent California drought as an extreme value. *Geophys. Res. Lett.* **42**, 6771–6779 (2015).
16. Serna, J. California faces $860-million repair bill for roads battered by record winter storms. *Los Angeles Times* (3 April 2017).
17. Schmidt, S., Hawkins, D & Phillips, K. 188,000 evacuated as California's massive Oroville Dam threatens catastrophic floods. *Washington Post* (3 February 2017).
18. Seager, R. et al. Causes of the 2011–14 California drought. *J. Clim.* **28**, 6997–7024 (2015).
19. Simpson, I. R., Seager, R., Ting, M. & Shaw, T. A. Causes of change in Northern Hemisphere winter meridional winds and regional hydroclimate. *Nat. Clim. Change* **6**, 65–70 (2016).
20. Neelin, J. D., Langenbrunner, B., Meyerson, J. E., Hall, A. & Berg, N. California winter precipitation change under global warming in the Coupled Model Intercomparison Project Phase 5 ensemble. *J. Clim.* **26**, 6238–6256 (2013).
21. Berg, N. & Hall, A. Increased interannual precipitation extremes over California under climate change. *J. Clim.* **28**, 6324–6334 (2015).
22. Wang, S.-Y. S., Huang, W.-R. & Yoon, J.-H. The North American winter 'dipole' and extremes activity: a CMIP5 assessment. *Atmos. Sci. Lett.* **16**, 338–345 (2015).
23. Yoon, J.-H. Increasing water cycle extremes in California and in relation to ENSO cycle under global warming. *Nat. Commun.* **6**, 8657 (2015).
24. Dettinger, M. Climate change, atmospheric rivers, and floods in California—a multimodel analysis of storm frequency and magnitude changes. *J. Am. Water Resour. Assoc.* **47**, 514–523 (2011).
25. Giorgi, F. et al. Higher hydroclimatic intensity with global warming. *J. Clim.* **24**, 5309–5324 (2011).
26. Trenberth, K. E., Dai, A., Rasmussen, R. M. & Parsons, D. B. The changing character of precipitation. *Bull. Am. Meteorol. Soc.* **84**, 1205–1217 (2003).
27. Donat, M. G., Lowry, A. L., Alexander, L. V., Ogorman, P. A. & Maher, N. More extreme precipitation in the world's dry and wet regions. *Nat. Clim. Change* **6**, 508–513 (2016).
28. Diffenbaugh, N., Swain, D. & Touma, D. Anthropogenic warming has increased drought risk in California. *Proc. Natl Acad. Sci. USA* **112**, 3931–3936 (2015).
29. Williams, A. P. et al. Contribution of anthropogenic warming to California drought during 2012–2014. *Geophys. Res. Lett.* **42**, 6819–6828 (2015).
30. Wang, S. Y., Hipps, L., Gillies, R. R. & Yoon, J.-H. Probable causes of the abnormal ridge accompanying the 2013–2014 California drought: ENSO precursor and anthropogenic warming footprint. *Geophys. Res. Lett.* **41**, 3220–3226 (2014).
31. Swain, D. L. et al. Remote linkages to anomalous winter atmospheric ridging over the northeastern Pacific. *J. Geophys. Res. Atmos.* **122**, 12194–12209 (2017).
32. Angélil, O. et al. An independent assessment of anthropogenic attribution statements for recent extreme temperature and rainfall events. *J. Clim.* **30**, 5–16 (2017).
33. IPCC *Climate Change 2013: The Physical Science Basis* (eds Stocker, T. F. et al.) (Cambridge Univ. Press, 2013).
34. Kay, J. E. et al. The Community Earth System Model (CESM) Large Ensemble project: a community resource for studying climate change in the presence of internal climate variability. *Bull. Am. Meteorol. Soc.* **96**, 1333–1349 (2015).
35. Diffenbaugh, N. S. et al. Quantifying the influence of global warming on unprecedented extreme climate events. *Proc. Natl Acad. Sci. USA* **114**, 4881–4886 (2017).
36. Jakob, D. in *Extremes in a Changing Climate: Detection, Analysis and Uncertainty* (eds AghaKouchak, A., Easterling, D., Hsu, K., Schubert, S. & Sorooshian, S.) 363–417 (Springer, New York, 2013).
37. Ralph, F. M. et al. Flooding on California's Russian River: role of atmospheric rivers. *Geophys. Res. Lett.* **33**, L13801 (2006).
38. Engstrom, W. N. The California Storm of January 1862. *Quat. Res.* **46**, 141–148 (1996).
39. Porter, K. et al. *Overview of the ARkStorm Scenario* Report No. 2010-1312 (United States Geological Survey, 2011).
40. Wing, I. S., Rose, A. Z. & Wein, A. M. Economic consequence analysis of the ARkStorm scenario. *Nat. Hazards Rev.* **17**, A4015002 (2016).
41. Jones, C., Waliser, D. E., Lau, K. M. & Stern, W. Global occurrences of extreme precipitation and the Madden–Julian Oscillation: observations and predictability. *J. Clim.* **17**, 4575–4589 (2004).
42. Hoell, A. et al. Does El Niño intensity matter for California precipitation? *Geophys. Res. Lett.* **43**, 819–825 (2016).
43. Diffenbaugh, N. S. & Giorgi, F. Climate change hotspots in the CMIP5 global climate model ensemble. *Climatic Change* **114**, 813–822 (2012).
44. Teng, H. & Branstator, G. Causes of extreme ridges that induce California droughts. *J. Clim.* **30**, 1477–1492 (2016).
45. Trenberth, K. E., Dai, A., Rasmussen, R. M. & Parsons, D. B. The changing character of precipitation. *Bull. Am. Meteorol. Soc.* **84**, 1205–1217 (2003).
46. Cvijanovic, I. et al. Future loss of Arctic sea-ice cover could drive a substantial decrease in California's rainfall. *Nat. Commun.* **8**, 1947 (2017).
47. Lee, M.-Y., Hong, C.-C. & Hsu, H.-H. Compounding effects of warm sea surface temperature and reduced sea ice on the extreme circulation over the extratropical North Pacific and North America during the 2013–2014 boreal winter. *Geophys. Res. Lett.* **42**, 1612–1618 (2015).
48. Blackport, R. & Kushner, P. J. Isolating the atmospheric circulation response to Arctic sea ice loss in the coupled climate system. *J. Clim.* **30**, 2163–2185 (2017).

Acknowledgements

Author contributions

D.L.S., B.L., J.D.N, and A.H. conceived of the study and designed the analyses. D.L.S. and B.L. provided analysis tools and conducted the analyses. D.L.S. wrote the manuscript and B.L., J.D.N. and A.H. provided comments and feedback.

Competing interests

The authors declare no competing interests.

Additional information

Methods

Datasets used in this study. The CESM-LENS is a large ensemble of fully coupled model simulations designed to explore multiple realizations of internal climate system variability on long timescales. We used precipitation output from an 1,800 year PIC run and 40 separate simulations of the twentieth century (20C; 1920–2005) and RCP8.5 (2005–2100) climate change scenario[49]. Each of the 40 20C + RCP8.5 realizations is generated using the same climate model but with slightly perturbed initial conditions, which yield different time sequences of daily- to decadal-scale internal variability[50]. Thus, CESM-LENS offers an opportunity to examine robust changes in extreme events across a wide range of simulated internal variability—a considerable advantage relative to other investigations that have historically been limited by the shortness of the observational record and the relative infrequency of extreme hydroclimatic events in smaller ensembles.

We also used precipitation output from climate model simulations generated as part of the CMIP5 project[49] for comparison with CESM-LENS simulations. We constructed a multi-model ensemble consisting of 78 realizations from 35 distinct climate models, where each distinct model receives equal weight in the ensemble mean and fields are interpolated to a common 2.5° grid.

We used the National Climatic Data Center's nClimDiv observational divisional dataset to determine the relative rank of historical precipitation events to estimate approximate return intervals (Supplementary Fig. 2). Existing biases between simulated and observed precipitation were implicitly accounted for using the methodology described below. Finally, we used gridded observational precipitation data to validate CESM-LENS precipitation (see section on Suitability of CESM-LENS for simulating California precipitation).

Quantifying changes in frequency of extreme hydroclimatic events. We seek to quantify changes in the frequency of extreme wet, dry and whiplash events in a manner that implicitly accounts for model biases and sidesteps parametric assumptions regarding the underlying shape of the precipitation distribution. In doing so, we focus on relative changes in the frequency of occurrence of events exceeding fixed thresholds defined using the PIC simulation. PIC atmospheric greenhouse gas concentrations are maintained at constant levels similar to those before the start of the Industrial Revolution (that is, year 1850 levels)—representing a counterfactual climate without human influence. We subsequently compare the relative change in frequency of specific events in the 20C + RCP8.5 simulations. The 20C forcing includes rising greenhouse gas and aerosol concentrations close to those observed in the historical record, and RCP8.5 forcing includes projected greenhouse gas increases between 2005 and 2100 based on a business-as-usual emissions trajectory[49]. We examine the RCP8.5 simulations as they most closely resemble the observed emissions trajectory to date[51], and they provide a larger signal-to-noise ratio for statistically rare extreme events[52].

We restrict our analysis of extremes to the months of November to March, representing the peak of the California rainy season[14]. While the seasonal peak of monthly precipitation occurs earlier in Northern California than in Southern California, extreme winter-like precipitation events associated with mid-latitude cyclonic activity can occur during any of these calendar months throughout the state. Thus, data for November–March are pooled to create a single, spatially explicit rainy season distribution of precipitation accumulations in each grid box.

Using direct observational (and indirect historical) records, we first estimate the approximate return interval for each event of interest. Our definition of return interval (R) is consistent with that widely used in the climate and civil engineering literature[36]: the likelihood of occurrence in any given year of an event with an n year return interval is $1/n$. Using this fixed return interval, we then calculate the precipitation value (p) in the CESM-LENS PIC simulation that occurs with frequency $1/n$ at each climate model grid box. In the 40-member ensemble, we then count exceedances of the specific return values and normalize the PIC and 20C + RCP8.5 runs on an events-per-year basis.

Once these counts are tabulated across all ensemble members and each season, we calculate percent changes in the frequency F of a given event at time t relative to the PIC period:

$$\Delta F_t = \frac{F_t - F_{PIC}}{F_{PIC}} \qquad (1)$$

This approach is modelled after ref. [35] and references therein. We note that our use of a fixed return interval, rather than percentile values, allows us to directly compare precipitation extremes spanning timescales from monthly to multi-annual. For example: the 98th percentile of daily precipitation might be expected to occur several days per year, but the 98th percentile of annual precipitation might be expected to occur only twice per century.

Definition of precipitation whiplash. Given the potential for adverse human impacts of rapid transitions between dry and wet conditions in California (as occurred during 2016–2017), we formalize two precipitation whiplash metrics across a range of timescales. We define year-to-year (interannual) whiplash years to be those during which seasonal (November–March) precipitation accumulation meets or exceeds the PIC 80th percentile and which were immediately preceded by a year with seasonal precipitation at or below the PIC 20th percentile. We define

within-season (intraseasonal) whiplash as the standard deviation of monthly precipitation within individual rainy seasons across the ensemble.

Selection of extreme events and climate model analogues. *2016–2017 (wet) analogue with 25 year return interval.* This threshold is based on the extremely wet 2016–2017 winter, during which record wet seasonal precipitation (return interval > 100 years) occurred across portions of Northern California and relatively smaller positive anomalies occurred over Southern California (return interval ~10 years), yielding a mean statewide return interval of approximately 15–25 yr for November–March. Given the strong latitudinal gradient in relative abnormality of seasonal precipitation during this period—and the consequent variation in adverse societal impacts across the state—we use a 25 yr return interval as a compromise threshold.

1861–1862 (wet) analogue with 200 year return interval. This threshold is based on the extraordinary sequence of atmospheric river storm events that brought extremely severe and widespread flooding to much of California during the 1861–1862 winter. Much of what is known about the 'Great Flood of 1862' has been pieced together from informal historical accounts and newspaper records from the then-nascent State of California[38,52]. Such records suggest that the most intense period of nearly continuous precipitation occurred between late December 1861 and late January 1862 over an approximately 40 day period, yielding rainfall accumulations over 1 m in some locations[38]. While this event occurred before the advent of reliable meteorological observations in California, palaeoclimate evidence from sediment records in coastal river systems suggests that events comparable to the 1861–1862 flood are associated with an approximately 200 year return interval[53]. Given the substantial uncertainties regarding the exact duration, magnitude and recurrence interval of the 1861–1862 event, we define our analogue as the 40 day cumulative precipitation during all November–March periods with a return interval of 200 years in the PIC simulation. The magnitude of this event is larger than that envisioned in the 'ARkStorm' natural hazard contingency planning scenario jointly developed by the United States Geological Survey and the State of California[39] but smaller in magnitude compared with several other probable events in the past millennium[53].

Recent research has suggested that a modern recurrence of the 1861–1862 flood would probably have a catastrophic human and socioeconomic toll[39,40]. Thus, despite the fact that such an event remains unlikely in any given year even under strong greenhouse forcing, a multi-fold relative increase in physical event likelihood combined with a high degree of socioeconomic vulnerability collectively yield a substantial increase in the overall risk associated with such an event over a period of decades[54].

1976–1977 (dry) analogue with 100 year return interval. This threshold is based on the extremely dry conditions that occurred during winter 1976–1977, which was the driest such period in California's 122 year observational record. This short-lived but intense drought led to acute water shortages in regions dependent on surface runoff from smaller hydrological basins and without direct access to State Water Project or Central Valley Project reservoirs. We conservatively assume a 100 year return period for this single-year event analogue threshold.

2012–2016 (dry) analogue with 100 year return interval. This threshold is based on the multi-year drought that occurred in California between late 2012 and early 2016. A substantial fraction of overall drought magnitude and associated impacts can be attributed to extremely warm temperatures that coincided with the lack of precipitation during successive winters[28,29], and while 2013 was the driest calendar year on record in California[8], no individual November–March period was the drier than 1976–1977. Nevertheless, the driest consecutive 3 year period (and consecutive November–March seasons) on record in California did indeed occur between 2013 and 2016 (ref. [14]), and we use this 3-year threshold as a benchmark for a high-impact, multi-year drought. We emphasize that the widespread environmental impacts of this event were substantially exacerbated by record warm temperatures—which are expected to be a signature of future droughts in this region as the climate warms[28,55]. Consistent with the single-year dry event, we conservatively assume a 100 year return interval.

Quantification of statistical significance. All figures showing spatial changes (latitude–longitude and time–latitude maps) represent 30 year running means in the 20C + RCP8.5 simulations. In all significance assessments below, these 30 year mean changes in event frequency are compared with resampled (bootstrapped) time series from the PIC simulation. Confidence intervals represent climate change signals that fall outside the sampled range of PIC variability with 90% confidence, representing a high statistical bar given the very wide range of simulated internal variability that exists within CESM-LENS[50].

Change-in-frequency maps. To provide a robust measure of statistical significance for change-in-frequency maps (Figs. 1–4 and Supplementary Fig. 2), we used a bootstrap resampling approach. For seasonal extreme events (25 year wet events and 100 year dry events), we generated 10,000 random time series by selecting wet season precipitation totals from the full 1,800 year PIC run (with replacement).

The length of each time series corresponds to the return interval of the event itself: in this instance, either 25 or 100 years. Next, in each resampled time series, the number of exceedances of 25 or 100 year events was calculated and translated into a ratio relative to the full PIC count, producing a distribution of 10,000 bootstrapped ratio values at each grid point. Finally, these distributions were used to determine the rarity of the simulated ratios relative to internal variability in the PIC run. In all map plots, cross-hatching for wet (dry) events represent a value at or above (at or below) the 90th (10th) PIC percentile—signifying 90% confidence ($P < 0.1$) that ratios fall outside of the PIC internal variability. In time series plots shown in Figs. 1–4, error bars represent two-thirds of the spread ($\pm 33.3\%$) of 40 ensemble members, and the average is calculated on a 30 year running mean basis to distinguish long-term trends from interannual variability.

We used a modified version of the bootstrap resampling approach described above for the 200 year event change-in-frequency map (Fig. 2 and Supplementary Fig. 2). Given the computational constraint of large-N resampling using this dataset, 100 resampled time series were constructed for this particularly extreme event (we confirm that $N = 100$ is a sufficiently large sample size for estimates of precipitation values to stabilize). For each time series, 200 years were chosen at random (each of which contains a distribution of 40 day running sums of November–March precipitation). We note that temporal autocorrelation can become problematic when counting occurrences using 40 day running sums for high-magnitude events. To ensure that our frequency counts do not unintentionally count these extremes twice, our algorithm skips ahead by 40 days each time a 200-year-magnitude event is encountered. As for other extreme events, we calculated the ratio of event frequencies between the full PIC run and the bootstrapped time series at each grid point.

For change-in-frequency maps of seasonal whiplash events (Fig. 4a), 10,000 block bootstrapped time series were generated using randomly chosen segments of 100 consecutive years. This consecutive-year (block) approach is necessary because our whiplash definition depends on sequential dry-to-wet transitions; thus, to appropriately sample the internal variability, the underlying temporal sequence in the PIC simulation must be preserved.

For change-in-frequency maps of month-to-month precipitation variability (Supplementary Fig. 2c), P values are calculated using 10,000 bootstrapped 40 year time series of November–March PIC precipitation. In each bootstrap iteration, 40 years were selected at random and with replacement, and the standard deviation across 200 (40×5) November–March model months was calculated for comparison with the CESM-LENS 40-member ensemble. Distributions of these month-to-month variability measures were generated at each grid point and normalized by the full PIC run to represent ratios.

For time series plots referring to either Southern California or Northern California, we use a spatially smoothed mean value (defined as the average value within a 3×3 grid box cluster centred on the original CESM-LENS grid box closest to the actual latitude/longitude of Los Angeles and San Francisco, respectively).

Time–latitude plots. The bootstrapped time series discussed above are also used to calculate statistical significance for time–latitude plots. After these bootstrapped time series were generated, further calculations were completed using the average of three contiguous west-to-east-oriented grid boxes along the California coast at each relevant latitude. As before, P values <0.1 resulting from the significance test imply rejection of the null hypothesis that the ratios in the time–latitude plots are within the range of simulated internal variability in the PIC simulation. In the present case, rejection of the null hypothesis is interpreted to mean that the 20C + RCP8.5 distribution is statistically distinguishable from the 'climate without humans' control.

Analysis of large-scale atmospheric conditions linked to extremes. We created anomaly composite maps for 500 hPa geopotential heights (GPH; Fig. 6a,d) and column-integrated water vapour (Fig. 6c,f) for wet years (exceeding the 80th preindustrial percentile) and dry years (falling below the 20th percentile) in the LENS simulations during both the full 1,800 year PIC simulation and across the 40 ensemble members of the RCP8.5 simulation between 2081 and 2100 (yielding a sample size of 760 model years). To simplify visual comparison of the anomaly patterns (where spatial gradients determine the geostrophic wind field) a spatially constant component of the thermal dilation[5,14] of the atmosphere (Supplementary Fig. 8a) was removed by subtracting the field mean difference in GPH (RCP8.5 minus PIC for a broad region near California (20° N–60° N, 180° E–250° E) from all grid points before generating RCP8.5 anomaly fields (Fig. 6a,d). We also compare the difference in anomalies between the RCP8.5 and PIC for wet and dry years (Fig. 6b,c,e,f) to emphasize the relative similarity of the underlying atmospheric circulation features between these periods.

Suitability of CESM-LENS for simulating California precipitation. The majority of findings in this study were derived using a global climate model operating at relatively coarse spatial resolutions (nominally 1°, or ~100 km, for the CESM configuration in LENS[34]). Given the importance of fine-scale topography in influencing California precipitation extremes[6], the relative spatial coarseness of model data used in this study precludes quantitative estimates of future runoff volume and flood flows at the watershed scale. Indeed, we note that that a local

minimum in the relative increase in wet extremes exists along the axis of maximum topographic slope in the CESM-LENS boundary conditions (Supplementary Fig. 9b), suggesting a possible nonlinearity in orographic precipitation scaling with warming (a possibility supported by recent high-resolution modelling experiments, for example, ref. [56]). In the present study, however, our focus on relative (rather than absolute) changes in the frequency of various precipitation extremes across broad regions implicitly accounts for possible simulated precipitation biases arising from coarse model resolution and other sources.

We reiterate that CESM-LENS, while state-of-the-art, is a single-model ensemble. Substantial intermodel differences do exist in the simulated atmospheric response to anthropogenic forcing[7], but we have chosen to focus on results using exclusively CESM-LENS data for two reasons. First, CESM-LENS includes 40 ensemble members over a 180 year simulation (1920–2100)—yielding a very large (7,200-model year) sample size, allowing us to directly examine very rare extreme events (such as the '200 year flood') without making assumptions about the character of the underlying statistical distribution. Combining this with the 1,800 year PIC simulation allows for evaluation of very rare events that would otherwise not be possible in the observational record or CMIP5 experiments. Recent evidence suggests that (1) CESM reproduces both the mean and variability of observed California precipitation with reasonable fidelity[9] (Supplementary Fig. 10), (2) the CESM-LENS single-model ensemble mean lies close to the median of the CMIP5 multi-model ensemble mean in the vicinity of California (Supplementary Fig. 6) and (3) CESM reproduces remote teleconnections (that is, those associated with ENSO) critical to California precipitation[57] (Supplementary Fig. 11).

To independently confirm that CESM-LENS is an appropriate tool for investigating changes in California precipitation, we compare simulated versus observed precipitation distributions for the 20C historical period for Northern and Southern California. We perform this validation using a gridded observational dataset (the Global Precipitation Climatology Project (GPCP) version 2.3[58]). To generate distributions for Northern and Southern California regions (depicted as white boxes in Supplementary Fig. 9), we sum November–March precipitation over land-only grid boxes with centroids that fall within a 200 km radius of San Francisco and Los Angeles, respectively, during the 1980–2016 period of mutual overlap between the CESM-LENS 20C simulations and the GPCP dataset.

We find that despite slight positive bias in median seasonal precipitation (<5% for Southern California and +9% for Northern California), the overall shape of the CESM-LENS distribution for both regions is statistically indistinguishable from observations at the 5% level using a Kolgoromov–Smirnoff test (Supplementary Fig. 10). We note that the CESM-LENS distribution tends to have slightly longer tails than observations, but this is unsurprising given that the effective sample size of the historical simulation (1,440 model years) is much larger than for the observational dataset (40 years) and the range of distribution among the 40 realizations encompasses the GPCP data (see horizontal bars in Supplementary Fig. 10). As our overall methodology implicitly accounts for mean biases in precipitation, and our focus is on extreme events in the upper and lower tails of the distribution, the outcome of this validation exercise strongly suggests CESM-LENS is capable of capturing both the median and underlying interannual variability of California hydroclimate.

Having confirmed these measures of fidelity of simulated California precipitation in CESM-LENS relative to observations, we assess whether the ensemble also captures the large-scale physical processes and teleconnections responsible for precipitation variability in this region. To test whether CESM-LENS plausibly reproduces the observed ENSO teleconnection, we perform linear regression of 500 hPa GPH on sea surface temperatures in the 'Nino3.4' region of the tropical eastern Pacific Ocean using data from both CESM-LENS and National Centers for Environmental Prediction/National Center for Atmospheric Research (NCEP/NCAR) R1[59]. The spatial pattern of the GPH teleconnection is substantially similar between CESM-LENS simulations and the R1 reanalysis (corroborating results previously shown in ref. [57]), and is characterized by a deepening of North Pacific low pressure and a more modest decrease in mid-tropospheric heights eastward over California and the southern tier of the United States (Supplementary Fig. 11a,b) during El Niño events. We further confirm that the mean position and magnitude of the cool-season (November–March) jetstream is close to that in observations (Supplementary Fig. 11b,c), though we also point out that even subtle biases could potentially lead to latitudinal shifts in the location of precipitation extreme changes discussed here (an issue that has been raised in previous work[60]). Finally, the large-scale atmospheric circulation patterns during California wet and dry years, respectively, exhibit similar spatial patterns and magnitudes to those observed during historical wet and dry years (Supplementary Fig. 12), especially in key regions near the US West Coast. Collectively, these results suggest that CESM-LENS is an appropriate tool for use in characterizing changes in regional precipitation extremes in the vicinity of California.

Code availability. The code used in the analyses described in this study is available from the corresponding author upon reasonable request.

Data availability. Precipitation data from the CESM-LENS simulations are available from the University Corporation for Atmospheric Research (http://www.

cesm.ucar.edu/projects/community-projects/LENS/data-sets.html). Precipitation data for California are available from the National Oceanic and Atmospheric Administration National Climatic Data Center (nClimDiv, www.ncdc.noaa.gov/monitoring-references/maps/us-climate-divisions.php) and National Oceanic and Atmospheric Administration Earth System Research Laboratory (NOAA ESRL) (GPCP, https://www.esrl.noaa.gov/psd/data/gridded/data.gpcp.html). CMIP5 ensemble data were obtained from Lawrence Livermore National Laboratory's Earth System Grid portal (https://esgf.llnl.gov) via the Royal Netherlands Meteorological Institute Climate Explorer (https://climexp.knmi.nl). Geopotential height and wind data from NCEP/NCAR R1 are available from NOAA ESRL (https://www.esrl.noaa.gov/psd/data/gridded/data.ncep.reanalysis.html) and additional composite data were created using the NOAA ESRL plotting tool (https://www.esrl.noaa.gov/psd/cgi-bin/data/composites/printpage.pl).

References

49. Taylor, K. E., Stouffer, R. J. & Meehl, G. A. An overview of CMIP5 and the experiment design. *Bull. Am. Meteorol. Soc.* **93**, 485–498 (2012).
50. Deser, C., Phillips, A. S., Alexander, M. A. & Smoliak, B. V. Projecting North American climate over the next 50 years: uncertainty due to internal variability. *J. Clim.* **27**, 2271–2296 (2014).
51. Fuss, S. et al. Betting on negative emissions. *Nat. Clim. Change* **4**, 850–853 (2014).
52. Dettinger, M.D. & Ingram, B.L. The coming megafloods. *Sci. Am.* **308**, 64–71 (2012).
53. Malamud-Roam, F. P., Lynn Ingram, B., Hughes, M. & Florsheim, J. L. Holocene paleoclimate records from a large California estuarine system and its watershed region: linking watershed climate and bay conditions. *Quat. Sci. Rev.* **25**, 1570–1598 (2006).
54. IPCC *Managing the Risks of Extreme Events and Disasters to Advance Climate Change Adaptation* (eds Field, C.B. et al.) (Cambridge Univ. Press, 2012).
55. Overpeck, J. T. The challenge of hot drought. *Nature* **503**, 350–351 (2013).
56. Sandvik, M. I., Sorteberg, A. & Rasmussen, R. Sensitivity of historical orographically enhanced extreme precipitation events to idealized temperature perturbations. *Clim. Dynam.* **50**, 143–157 (2018).
57. Allen, R. J. & Luptowitz, R. El Niño-like teleconnection increases California precipitation in response to warming. *Nat. Commun.* **8**, 16055 (2017).
58. Adler, R. F. et al. The Version-2 Global Precipitation Climatology Project (GPCP) monthly precipitation analysis (1979–present). *J. Hydrometeorol.* **4**, 1147–1167 (2003).
59. Kalnay, E. et al. The NCEP/NCAR 40-year reanalysis project. *Bull. Am. Meteorol. Soc.* **77**, 437–471 (1996).
60. Hagos, S. M., Leung, L. R., Yoon, J.-H., Lu, J. & Gao, Y. A projection of changes in landfalling atmospheric river frequency and extreme precipitation over western North America from the Large Ensemble CESM simulations. *Geophys. Res. Lett.* **43**, 1357–1363 (2016).